EUROPEAN JOURNAL OF PURE AND APPLIED MATHEMATICS
2026, Vol. 19, Issue 2, Article Number 7795
ISSN 1307-5543 – ejpam.com
Published by New York Business Global

Nonlinear Identifiability and Critical Transitions in a Model of School Bullying Dynamics

Maryam Alamil[1], Ramazan Tinaztepe[1], Salih Tatar[1,*]

[1] *Department of Mathematics and Computer Science, College of Science and General Studies, Alfaisal University, Riyadh, KSA.*

Abstract. In this paper, we investigate nonlinear identifiability and critical transitions in a compartmental model of school bullying dynamics through three inverse problems: parameter estimation, reconstruction of initial conditions, and their joint identification from observational data. The problems are formulated as nonlinear least-squares tasks and solved using forward simulations combined with multi-start optimization. Numerical results show accurate recovery in the noise-free case and reasonable robustness under noise. However, identifiability strongly depends on the dynamical regime. In particular, near the critical threshold $R_0 \approx 1$, the system exhibits dynamical indistinguishability, where different parameter configurations produce similar observable trajectories. This reflects a loss of practical identifiability associated with critical transitions. The study highlights both the effectiveness and the intrinsic limitations of inverse problem approaches in nonlinear dynamical systems.

2020 Mathematics Subject Classifications: 34A55, 65L09, 65M32, 91D30, 97M70

Key Words and Phrases: Bullying dynamics, inverse Problem, multi-start optimization

1. Introduction

In this paper, we consider the following model for bullying dynamics introduced in [1]:

$$\begin{cases} \dfrac{ds}{dt} = -\beta s(t)b(t) - \alpha s(t)b(t) + \gamma b(t) + \varepsilon e(t), \\ \dfrac{db}{dt} = \alpha s(t)b(t) - \gamma b(t), \\ \dfrac{de}{dt} = \beta s(t)b(t) - \delta e(t) + \lambda v(t) - \varepsilon e(t), \\ \dfrac{dv}{dt} = \delta e(t) - \lambda v(t), \end{cases} \tag{1.1}$$

*Corresponding Author.
DOI: https://doi.org/10.29020/nybg.ejpam.v19i2.7795

Email addresses: `malamil@alfaisal.edu` (M. Alamil)
`rtinaztepe@alfaisal.edu` (R. Tinaztepe), `statar@alfaisal.edu` (S. Tatar)

where $s(t)$, $b(t)$, $e(t)$, and $v(t)$ denote the proportions of susceptible, bully, exposed, and violent individuals at time t, respectively.

We also note that system (1.1) conserves the total population, since $\frac{d}{dt}(s(t) + b(t) + e(t) + v(t)) = 0$, and hence $s(t) + b(t) + e(t) + v(t) = 1$ for all $t \geq 0$ provided that $s(0) + b(0) + e(0) + v(0) = 1$.

The susceptible class includes individuals not currently involved in bullying, including those who have never been bullied, those who were bullied in the past but have recovered, and those who previously engaged in bullying but have stopped. The bully class represents individuals actively engaging in bullying behavior. The exposed class consists of bullying victims who do not respond violently, whereas the violent class consists of bullied individuals who react through violent behavior.

The parameters $\alpha, \beta, \gamma, \delta, \lambda, \varepsilon$ are nonnegative constants describing the transition mechanisms between these compartments. The parameter α represents the rate at which susceptible individuals become bullies through contact, while β describes the transition from susceptible to exposed individuals. The parameter γ denotes the rate at which bullies cease their behavior and return to the susceptible class, reflecting the effect of interventions. Similarly, ε is the recovery rate of exposed individuals. The parameter δ models the escalation from exposure to violent behavior, and λ represents the de-escalation from violent to exposed individuals. Thus, α and β govern contact-driven transitions, while γ, ε, δ, and λ describe recovery, escalation, and de-escalation processes. For the mathematical analysis of system (1.1), including existence, uniqueness, and stability of solutions, we refer to [2].

Bullying has been widely studied in the educational, psychological, and public health literature, where it is generally defined as repeated aggressive behavior involving an imbalance of power between individuals. A substantial body of empirical research has documented its high prevalence in school environments and its significant short- and long-term consequences for both victims and perpetrators [3–7]. These studies consistently report strong associations between bullying involvement and adverse outcomes such as anxiety, depression, behavioral problems, and reduced academic performance [8–11]. Beyond individual-level effects, bullying has also been shown to negatively impact the overall school climate and peer relationships, highlighting its broader social implications [12–14]. Recent years have seen the emergence of cyberbullying and evolving social dynamics, further intensifying concern, with contemporary studies emphasizing the increasing prevalence and complexity of bullying behaviors [15, 16]. Earlier foundational work has also highlighted the persistence of bullying-related outcomes and the effectiveness of intervention strategies [17]. In parallel, there has been growing interest in modeling bullying dynamics using quantitative and mathematical frameworks, often drawing analogies with epidemiological processes to better understand the spread and persistence of aggressive behaviors within structured populations [18]. These contributions collectively underscore the importance of developing rigorous mathematical and statistical models to capture the underlying mechanisms of bullying and to inform effective prevention and intervention strategies. While the forward model has been studied in the literature, the inverse problems associated with parameter and initial-state reconstruction have not been systematically investigated. Building on this line of research, the present study further develops quantitative models of bullying dynamics by examining the underlying mechanisms and the role of key transition processes in school environments.

The novelty of this work lies in the integration of inverse problem methodology with nonlinear dynamical analysis in the context of social behavior modeling. Unlike existing studies that primarily focus on forward simulations of bullying dynamics, the present study systematically investigates the identifiability of both model parameters and initial conditions under different dynamical regimes. In particular, we show that the ability to recover unknown quantities is not uniform, but strongly depends on the qualitative behavior of the system. This leads to the identification of a nonlinear phenomenon in which critical transitions, especially near the threshold $R_0 \approx 1$, induce a form of dynamical indistinguishability, where different parameter configurations produce nearly identical observable dynamics. This perspective provides new insight into the limitations of data-driven inference in nonlinear systems and highlights the role of regime-dependent identifiability in complex social dynamics.

Motivated by recent advances in quantitative modeling of bullying dynamics, this study addresses the inverse analysis of a compartmental model in which key parameters and initial conditions are not directly observable and must be inferred from data. We consider three inverse problems: parameter estimation, reconstruction of initial conditions, and their joint identification. These problems are formulated as nonlinear least-squares optimization tasks and solved numerically through forward simulations combined with multi-start optimization to mitigate local minima. Numerical experiments are conducted under bullying-free, threshold, and endemic regimes, and across different noise levels. The results show that the proposed approach achieves accurate recovery in the noise-free case and maintains good robustness under moderate noise. However, they also reveal significant practical identifiability issues for certain parameter combinations, particularly near the critical threshold regime, where multiple parameter sets can produce similar system behavior. Overall, the present work shows that identifiability in inverse problems is not only a numerical issue, but a fundamentally dynamical property that depends on the qualitative regime of the underlying nonlinear system.

The remainder of the paper is organized as follows. In Section 2, we formulate the inverse problems. Section 3 describes the numerical methodology, including the least-squares reconstruction and computational strategy. Section 4 discusses the numerical results under different scenarios and noise levels, with emphasis on their practical implications.

2. Inverse Problem Formulation and Practical Motivation

In this section, we formulate the inverse problems considered in this work and discuss their practical relevance.

Inverse Problem 1 (IP1). Given the initial data

$$\begin{cases} s(0) = s_0, \\ b(0) = b_0, \\ e(0) = e_0, \\ v(0) = v_0, \end{cases} \tag{2.1}$$

and noisy measurements of $s(t)$, $b(t)$, $e(t)$, and $v(t)$ at observation times $t_1, \dots, t_m$, recover the constant transition-rate vector

$$\theta = (\alpha, \beta, \gamma, \varepsilon, \delta, \lambda),$$

such that the solution of (1.1) provides the best fit to the observed data.

Inverse Problem 2 (IP2). Given the transition-rate vector

$$\theta = (\alpha, \beta, \gamma, \varepsilon, \delta, \lambda),$$

and noisy measurements of $s(t)$, $b(t)$, $e(t)$, and $v(t)$ at observation times $t_1, \dots, t_m$, recover the initial-state vector

$$u_0 = (s_0, b_0, e_0, v_0), \tag{2.2}$$

under the constraints

$$s_0 \geq 0, \quad b_0 \geq 0, \quad e_0 \geq 0, \quad v_0 \geq 0, \quad s_0 + b_0 + e_0 + v_0 = 1, \tag{2.3}$$

such that the corresponding solution of (1.1) best fits the observed data.

Inverse Problem 3 (IP3). In a more realistic setting, both the transition-rate vector and the initial conditions are unknown. Given noisy observations of the state variables, the goal is to recover the augmented parameter vector

$$\theta = (\alpha, \beta, \gamma, \varepsilon, \delta, \lambda, s_0, b_0, e_0, v_0), \tag{2.4}$$

subject to the positivity conditions

$$\alpha, \beta, \gamma, \varepsilon, \delta, \lambda > 0, \tag{2.5}$$

and the constraint (2.3), so that the solution of (1.1) associated with θ best matches the available observations.

From an applied perspective, these inverse problems are of central importance because the key quantities governing bullying dynamics in schools are typically not directly observable. While schools may collect partial and noisy data on the proportions of susceptible, bullying, exposed, and violent individuals over time, the transition rates governing the spread of bullying behavior, recovery due to interventions, escalation to violence, and de-escalation processes remain unknown and must be inferred from data. In this context, IP1 is relevant for estimating the main behavioral and intervention-related rates, IP2 is useful when these rates are known or prescribed but the initial population distribution is uncertain and IP3 represents the most realistic situation in which both the transition mechanisms and the initial state must be identified simultaneously. Consequently, the study of these inverse problems is essential for model calibration, for linking the mathematical model with observable data, and for assessing the reliability of the reconstruction procedure in recovering practically meaningful information from noisy observations. We emphasize that the focus of this work is on computational identifiability and practical reconstruction rather than theoretical identifiability or uniqueness analysis.

3. Numerical Experiments

In this section, we present numerical experiments illustrating the solutions of the three inverse problems. Each inverse problem is solved by minimizing the following least-squares objective function

$$J(\theta) = \sum_i \|y(t_i;\theta) - y^{data}(t_i)\|^2, \tag{3.1}$$

where θ denotes the vector of unknowns in each inverse problem (i.e., model parameters, initial conditions, or both), and $\|\cdot\|$ is the Euclidean norm. The vector

$$y(t_i;\theta) = (s(t_i), b(t_i), e(t_i), v(t_i))$$

represents the solution of the ODE system corresponding to θ, while $y^{\text{data}}(t_i)$ denotes the observed data at time t_i.

The observed data $y^{data}(t_i)$ are generated by solving the ODE system using predetermined (true) values of θ (denoted by θ^{true}), and subsequently adding noise to mimic measurement uncertainty. The use of synthetic data allows controlled evaluation of reconstruction accuracy and identifiability, which is not possible with real-world data due to unknown ground truth. The particular θ that minimizes (3.1) will be denoted as $\widehat{\theta}$. This objective function simply measures the sum of squared differences between model predictions and observations at each time t_i. In the ideal noise-free case, if $\widehat{\theta} = \theta^{\text{true}}$, then $J(\widehat{\theta}) = 0$, indicating a perfect match between model and data.

The minimization of the function (3.1) involves two coupled tasks: finding the model solution $y(t_i;\theta)$, by solving the ODE system for each selection of θ and determining the optimal θ that minimizes the function J. These problems are solved by using MATLAB built-in solvers.

The forward problem is solved using the adaptive Runge–Kutta method implemented in the `ode45` solver, while the minimization of J is carried out using the nonlinear least-squares solver `lsqnonlin`. Since θ has several variables in each inverse problem, many local minima are expected. To mitigate the effect of local minima, the optimization is combined with the `MultiStart` strategy. To assess the performance of the inverse problem algorithms under different dynamical scenarios, we consider three representative parameter configurations determined by the relation between the parameters α and γ. Following [1], we use the threshold quantity

$$R_0 = \frac{\alpha}{\gamma} \tag{3.2}$$

to distinguish the three qualitative regimes considered in the numerical experiments. More precisely, for the model (1.1), the ratio α/γ governs the onset or decay of the bully class near the bullying-free state. Indeed, from

$$\frac{db}{dt} = \alpha s(t)b(t) - \gamma b(t),$$

and for initial stages with $s(t) \approx 1$, we obtain

$$\frac{db}{dt} \approx (\alpha - \gamma)b(t) = \gamma\left(\frac{\alpha}{\gamma} - 1\right) b(t).$$

Thus, $\alpha/\gamma > 1$ corresponds to initial growth of the bully population, whereas $\alpha/\gamma < 1$ corresponds to decay. This agrees with the equilibrium and stability analysis reported in [1], where $\alpha < \gamma$ yields the bullying-free regime and $\alpha > \gamma$ yields the endemic regime. When $\alpha \approx \gamma$ ($R_0 \approx 1$), the system operates near the threshold separating the bullying-free and endemic scenarios, and the dynamics become more sensitive to parameter variations. Accordingly, throughout this paper we use α/γ as the threshold quantity organizing the numerical experiments.

These three cases according to the threshold quantity allow us to evaluate the performance of the inverse algorithms under qualitatively different dynamical behaviors of the forward model. In particular, the experiments were carried out using $\alpha = 0.05$ for the bullying-free case, $\alpha = 0.40$ for the endemic case, and $\alpha = 0.20$ for the near-threshold case, while the remaining parameters were kept fixed, $\beta = 0.3$, $\gamma = 0.2$, $\varepsilon = 0.1$, $\delta = 0.05$, $\lambda = 0.07$. The initial conditions are chosen as $s(0) = 0.95, b(0) = 0.05, e(0) = 0, v(0) = 0$ consistent with the values presented in the study [1]. Note that these parameter values and initial conditions will be used as θ^{true} when generating the observed data. The following provides the technical setting for implementing the solvers in MATLAB. The system is simulated on the time interval $t \in [0, 150]$. Observation times were defined as $t_i = \text{linspace}(0, 150, 151)$. The observed data were generated by adding Gaussian noise to the model solution,

$$y^{data}(t_i) = y(t_i; \theta^{true}) + \zeta \cdot \mu_i,$$

where $\mu_i \sim \mathcal{N}(0,1)$ are independent standard normal random variables. The problems are solved for the noise levels, $\zeta = 0, \zeta = 0.02$ and $\zeta = 0.05$. In each inverse problem, the minimization problem was solved using the `lsqnonlin` algorithm with parameter bounds 10^{-6} and 2, that is, the components of θ can take the values in the interval $[10^{-6}, 2]$. To improve robustness against local minima, the optimization was repeated using the `MultiStart` procedure with 400 starting points, components of which are between 10^{-6} and 2. The choice of 400 starting points in the MultiStart procedure is heuristic and was made to balance robustness against local minima with computational cost; it should therefore be viewed as a practical numerical choice rather than a guarantee of global convergence. To evaluate the accuracy of the parameter estimation procedure, two quantitative measures were used: the value of J and the mean relative error (MRE). In addition, the accuracy of the recovered parameters is quantified using the mean relative error defined by

$$\text{MRE} = \frac{1}{|\Omega|} \sum_{k \in \Omega} \frac{|\widehat{\theta}_k - \theta_k^{true}|}{|\theta_k^{true}|},$$

where $\Omega = \{i : \theta_i \neq 0\}$ and $|\Omega|$ denotes its cardinality, θ_i^{true} are the true parameter values used to generate the synthetic data, and $\widehat{\theta}_k$ are the estimated parameters obtained from the inverse problem. We emphasize that the MRE is computed only over the index set $\Omega = \{k : \theta_k^{\text{true}} \neq 0\}$; therefore, components with zero true value are excluded from the sum. In particular, for the initial-condition reconstruction, the terms corresponding to $e_0^{\text{true}} = 0$ and $v_0^{\text{true}} = 0$ are omitted from $\text{MRE}(y_0)$. A smaller value of the mean relative error indicates a more accurate parameter recovery.

3.1. Inverse Problem 1

In IP1, all model parameters defined by $\theta = (\alpha, \beta, \gamma, \varepsilon, \delta, \lambda)$ are assumed to be unknown, while the initial values $s(0), b(0), e(0), v(0)$ are taken as $0.95, 0.05, 0, 0$ in accordance with the study [1]. Table 1 reports the results on a non-bullying case where $\alpha/\gamma = 0.25 < 1$ in θ^{true} with different noise levels. Table 2 reports the results on a threshold case where $\alpha/\gamma = 1$ in θ^{true} with different noise levels. Table 3 reports the results on an endemic case where $\alpha/\gamma = 2$ in θ^{true} with different noise levels.

We observe that, in the bullying-free and threshold cases, the parameter values are not accurately recovered when the observed data are noisy, with the mean relative error remaining relatively high. This behavior suggests that the inverse problem is practically ill-posed. To address this, we incorporated regularization into the objective function $J(\theta)$, including Tikhonov-type penalties on individual parameters as well as additional penalties on key dynamical combinations such as α/γ and $\alpha - \gamma$, motivated by the potential presence of correlated parameter effects. However, numerical experiments indicate that the inclusion of such regularization does not lead to a significant improvement in reconstruction accuracy or stability. Consequently, the results reported in this work are presented without regularization.

Table 1: Recovered parameters for **IP1** in the **bullying-free case** ($R_0 < 1$) (where $\alpha/\gamma < 1$ in θ^{true}) under different noise levels.

	Noise Level (θ):	0	0.02	0.05
Parameters (θ)	θ^{true}	$\widehat{\theta}$	$\widehat{\theta}$	$\widehat{\theta}$
α	0.05	0.054509	2.177923	1.580983
β	0.30	0.300020	0.324980	0.359459
γ	0.20	0.204249	2.160991	1.550111
ε	0.10	0.100016	0.170709	0.291169
δ	0.05	0.049997	0.056243	0.079898
λ	0.07	0.069998	0.089909	0.115622
$J(\theta)$	0	0.000000	0.0435092	0.2296809
MRE	0	0.02257238	8.76530238	6.60243333

Table 2: Recovered parameters **IP1** for the **threshold case** ($\alpha/\gamma \approx 1$ in θ^{true}) under different noise levels.

	Noise Level (θ):	0	0.02	0.05
Parameters (θ)	θ^{true}	$\widehat{\theta}$	$\widehat{\theta}$	$\widehat{\theta}$
α	0.20	0.20	0.160139	0.093437
β	0.30	0.30	0.324740	0.397120
γ	0.20	0.20	0.162256	0.098418
ε	0.10	0.10	0.117568	0.174086
δ	0.05	0.05	0.054424	0.072954
λ	0.07	0.07	0.080412	0.111904
$J(\theta)$	0	0	0.0758638	0.4056439
MRE	0	0	0.12451667	0.63261310

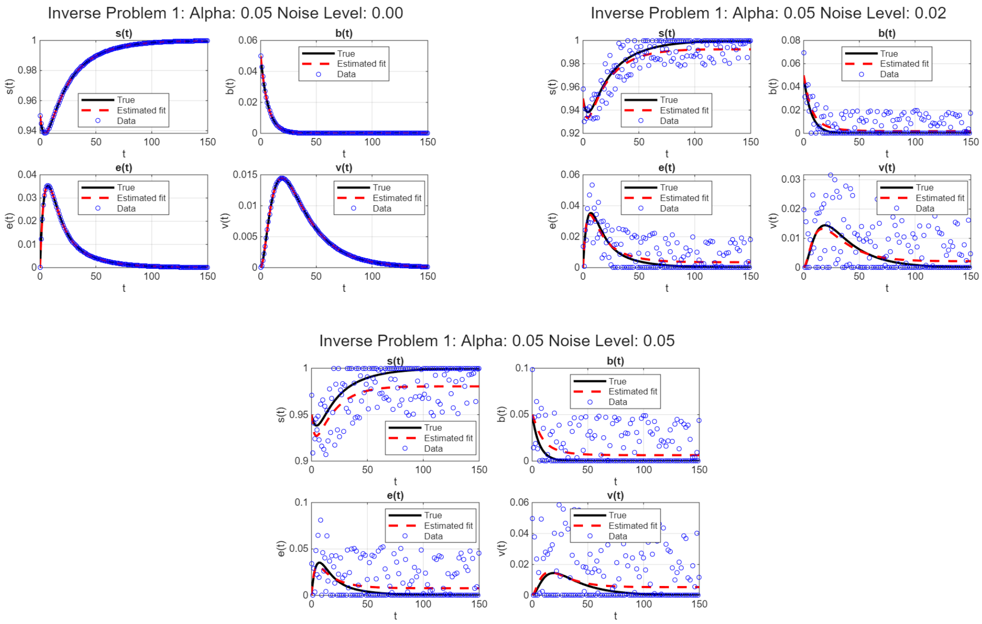

Figure 1: Numerical trajectories for **IP1** in the **non-bullying case** corresponding to the three noise levels $\zeta = 0$, 0.02, and 0.05.

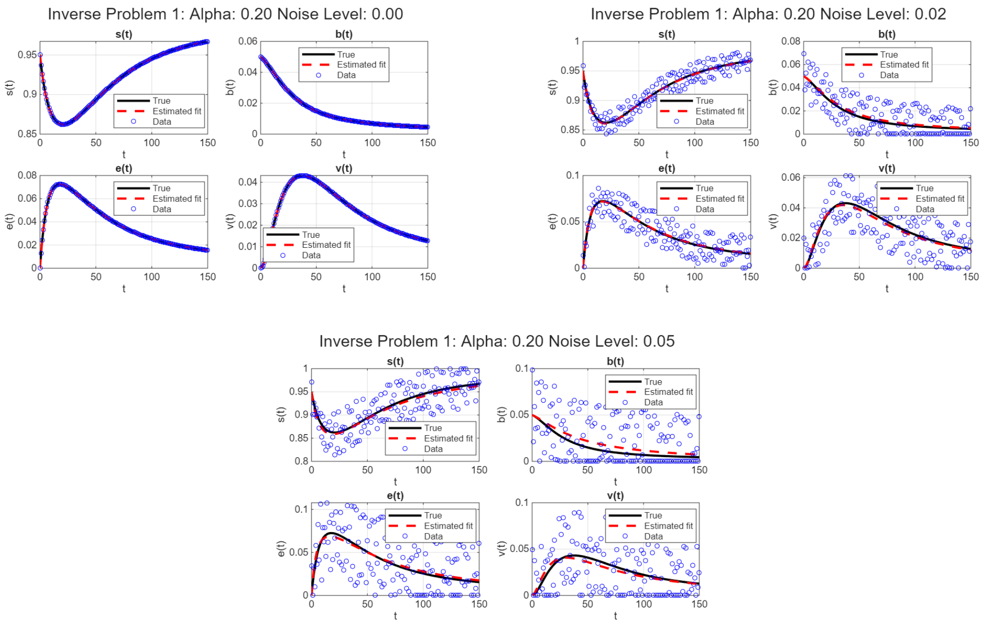

Figure 2: Numerical trajectories for **IP1** in the **threshold case** corresponding to the three noise levels $\zeta = 0$, 0.02, and 0.05.

Table 3: Recovered parameters **IP1** for the **endemic case** ($\alpha/\gamma > 1$) under different noise levels.

	Noise Level (θ):	0	0.02	0.05
Parameters (θ)	θ^{true}	$\widehat{\theta}$	$\widehat{\theta}$	$\widehat{\theta}$
α	0.40	0.40	0.405577	0.413928
β	0.30	0.30	0.296604	0.292020
γ	0.20	0.20	0.202655	0.206614
ε	0.10	0.10	0.099204	0.098167
δ	0.05	0.05	0.050485	0.051438
λ	0.07	0.07	0.071422	0.073936
$J(\theta)$	0	0	0.0809214	0.5043815
MRE	0	0	0.01517139	0.04044937

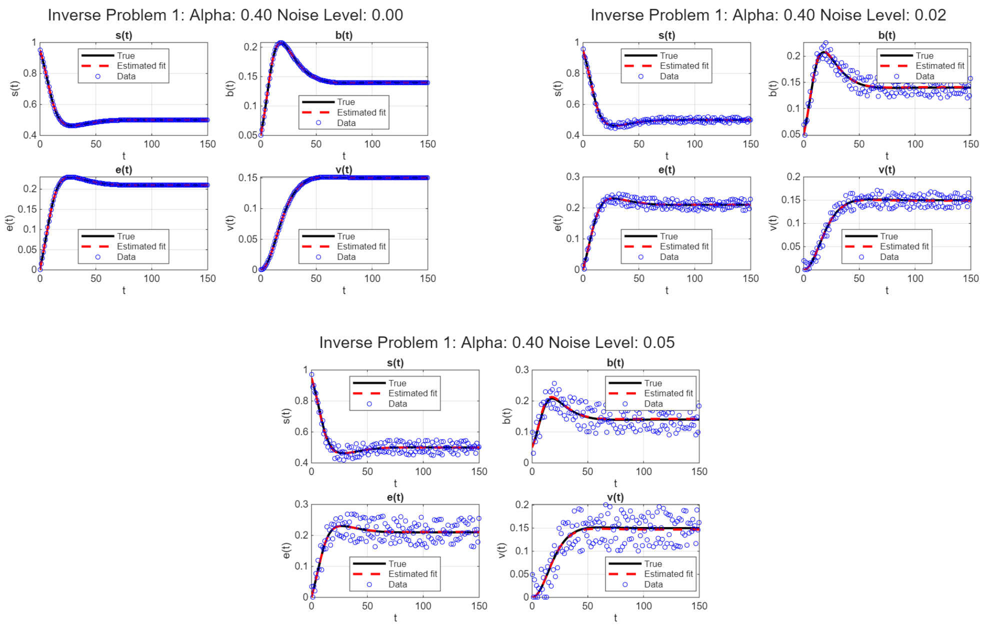

Figure 3: Numerical trajectories for **IP1** in the **endemic case** corresponding to the three noise levels $\zeta = 0$, 0.02, and 0.05.

3.2. Inverse Problem 2

In IP2, $\alpha, \beta, \gamma, \varepsilon, \delta, \lambda$ are assumed to be known while the initial state vector $u_0 = (s_0, b_0, e_0, v_0)$ is unknown and must be estimated. The objective function (3.1) is formulated accordingly, and the same numerical estimation procedure described in the previous section is applied. Table 4 reports the non-bullying case where $\alpha = 0.05$ and the rest is fixed as before. Table 5 reports the non-bullying case where $\alpha = 0.2$ and the rest is fixed as before. Table 6 reports the non-bullying case where $\alpha = 0.4$ and the remaining parameters are fixed as before.

Table 4: Recovered initial conditions in **IP2** for **non-bullying case** (where $\alpha/\gamma < 1$ in θ^{true}) under different noise levels.

	Noise Level:	0	0.02	0.05
Initial Conditions (y_0)	θ^{true}	$\widehat{\theta}$	$\widehat{\theta}$	$\widehat{\theta}$
s_0	0.95	0.95	0.945674	0.933173
b_0	0.05	0.05	0.050756	0.053657
e_0	0	0	0.000002	0.000000
v_0	0	0	0.003568	0.013170
$J(\theta)$	0	0	0.0494346	0.2738868
MRE	0	0	0.00983684	0.04542632

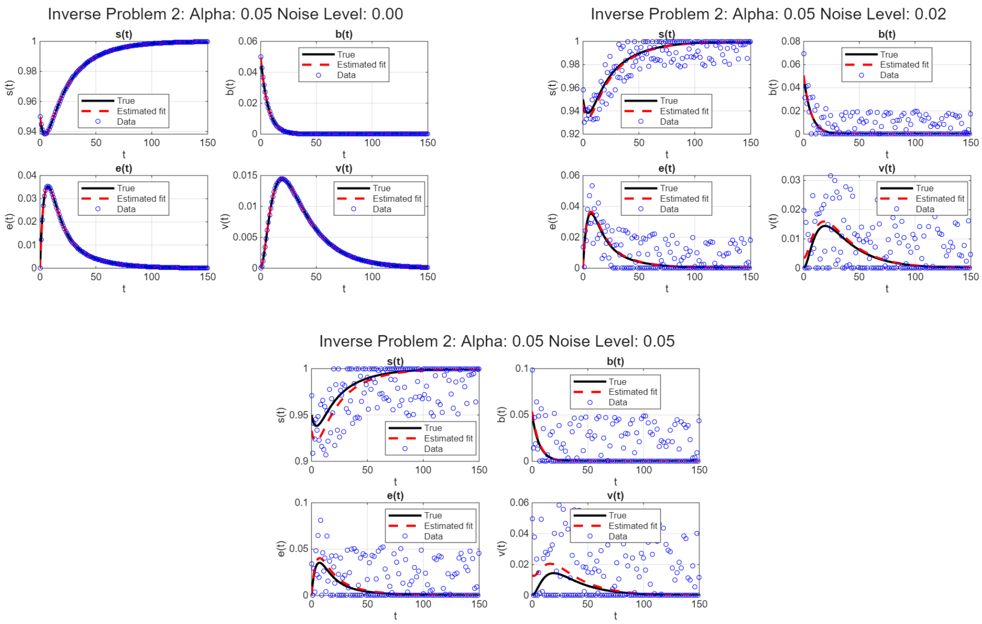

Figure 4: Numerical trajectories for **IP2** in the **non-bullying case** corresponding to the three noise levels $\zeta = 0$, 0.02, and 0.05.

Table 5: Recovered initial conditions in **IP2** for **threshold** (where $\alpha/\gamma \approx 1$ in θ^{true}) under different noise levels.

	Noise Level:	0	0.02	0.05
Initial Conditions (y_0)	θ^{true}	$\widehat{\theta}$	$\widehat{\theta}$	$\widehat{\theta}$
s_0	0.95	0.95	0.947605	0.943637
b_0	0.05	0.05	0.050459	0.051732
e_0	0	0	0.000000	0.000000
v_0	0	0	0.001937	0.004630
$J(\theta)$	0	0	0.07649945	0.413639
MRE	0	0	0.00585053	0.02066895

Table 6: Recovered initial conditions in **IP2** for **endemic** (where $\alpha/\gamma > 1$ in θ^{true}) under different noise levels.

	Noise Level:	0	0.02	0.05
Initial Conditions (y_0)	θ^{true}	$\widehat{\theta}$	$\widehat{\theta}$	$\widehat{\theta}$
s_0	0.95	0.95	0.948354	0.945126
b_0	0.05	0.05	0.050800	0.052042
e_0	0	0	0.000000	0.000000
v_0	0	0	0.000846	0.002832
$J(\theta)$	0	0	0.0812344	0.5062488
MRE	0	0	0.00886632	0.02298526

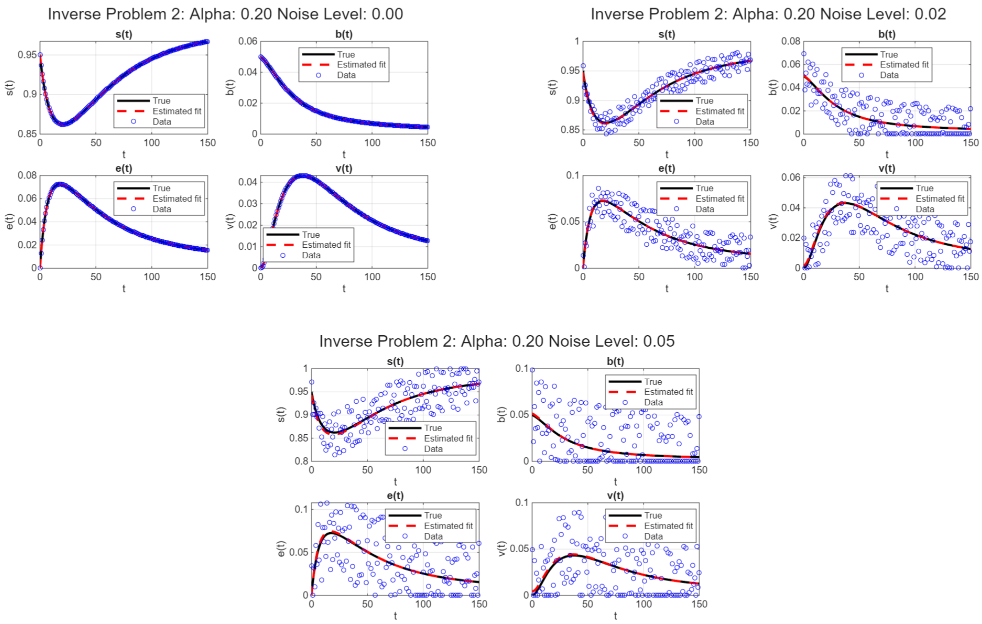

Figure 5: Numerical trajectories for **IP2** in the **threshold case** corresponding to the three noise levels $\zeta = 0$, 0.02, and 0.05.

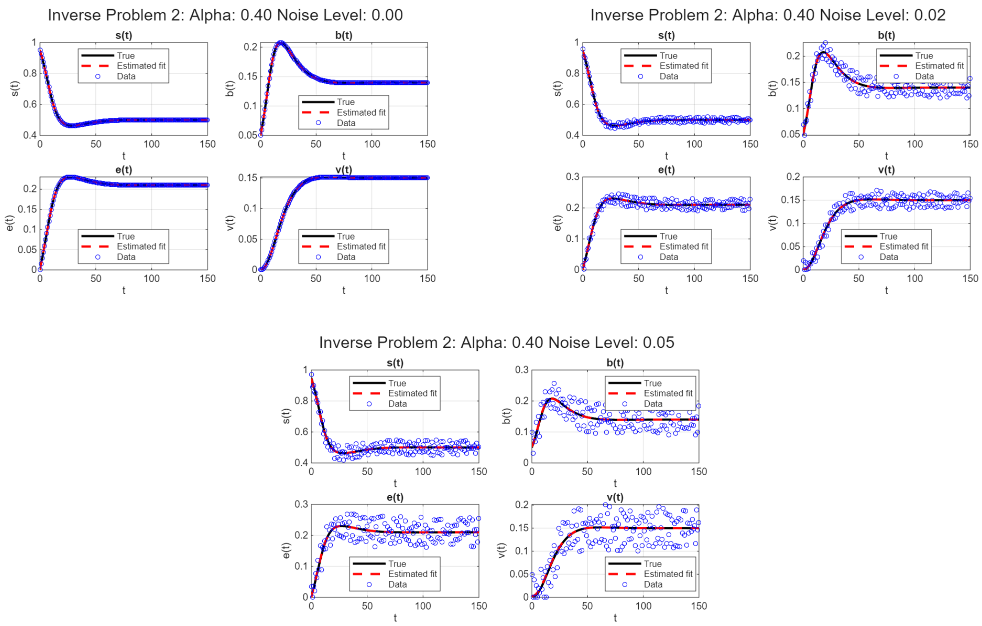

Figure 6: Numerical trajectories for **IP2** in the **endemic case** corresponding to the three noise levels $\zeta = 0$, 0.02, and 0.05.

3.3. Inverse Problem 3

In IP3, both the model parameters and the initial conditions are unknown. The function given by 3.1 is minimized to estimate θ. Table 7 gives the results on a non-bullying case where $\alpha/\gamma = 0.25 < 1$ in θ^{true} with different noise levels. Table 8 gives the results on a threshold case where $\alpha/\gamma = 1$ in θ^{true} with different noise levels. Table 9 gives the results on an endemic case where $\alpha/\gamma = 2$ in θ^{true} with different noise levels. As expected, this inverse problem is more challenging than IP1 and IP2, since both parameters and initial conditions must be identified simultaneously. The large values of the mean relative error (MRE) observed for the initial conditions are primarily due to the presence of zero true values. In such cases, even small absolute deviations lead to disproportionately large relative errors, which can overestimate the actual reconstruction error. Therefore, the MRE should be interpreted with caution when true parameter values are close to or equal to zero.

To assess the sensitivity to the number of starting points, we repeated representative experiments using 400 and 1000 MultiStart initializations. The results indicate that increasing the number of starting points does not remove the optimization difficulties in the threshold regime, suggesting that the limitation is intrinsic to the optimization landscape rather than caused only by insufficient sampling. Since the runs with 1000 starting points yielded qualitatively similar results and did not materially affect the conclusions, we do not report them in detail.

Table 7: Recovered parameters and initial conditions in **IP3** for **non-bullying case** (where $\alpha/\gamma < 1$ in θ^{true}) under different noise levels.

		Noise Level:	0	0.02	0.05
	$\theta = (\eta, y_0)$	θ^{true}	$\widehat{\theta}$	$\widehat{\theta}$	$\widehat{\theta}$
η	α	0.05	0.055924	2.107597	1.439630
	β	0.30	0.300034	0.307656	0.270810
	γ	0.20	0.205576	2.091394	1.411517
	ε	0.10	0.100024	0.163754	0.224046
	δ	0.05	0.049995	0.042378	0.043204
	λ	0.07	0.069995	0.073253	0.072217
y_0	s_0	0.95	0.950002	0.946612	0.937955
	b_0	0.05	0.049998	0.047765	0.044879
	e_0	0.00	0.000000	0.000000	0.003615
	v_0	0.00	0.000000	0.005623	0.013551
	$J(\theta)$	0	0.000000	0.0433311	0.228423
	MRE (η)	0	0.024481	8.578480	5.892589
	MRE (y_0)	0	0.000021	0.024133	0.057549

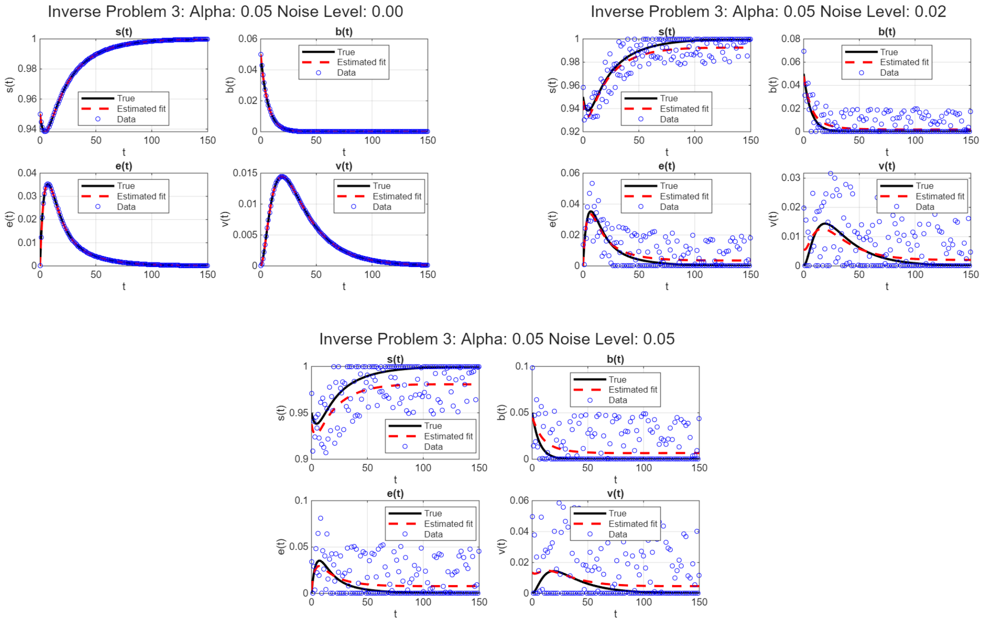

Figure 7: Numerical trajectories for **IP3** in the **non-bullying case** corresponding to the three noise levels $\zeta = 0$, 0.02, and 0.05.

Table 8: Recovered parameters and initial conditions in **IP3** for **threshold case** (where $\alpha/\gamma \approx 1$ in θ^{true}) under different noise levels.

		Noise Level:	0	0.02	0.05
	$\theta = (\eta, y_0)$	θ^{true}	$\widehat{\theta}$	$\widehat{\theta}$	$\widehat{\theta}$
η	α	0.20	1.362417	0.173033	0.119491
	β	0.30	0.259976	0.298116	0.313848
	γ	0.20	1.275472	0.174308	0.122577
	ε	0.10	0.026114	0.108666	0.141472
	δ	0.05	0.374016	0.052629	0.064020
	λ	0.07	0.544811	0.077867	0.098677
y_0	s_0	0.95	0.949742	0.946099	0.938934
	b_0	0.05	0.046316	0.051643	0.053810
	e_0	0.00	0.003941	0.000000	0.000000
	v_0	0.00	0.000000	0.002258	0.007257
	$J(\theta)$	0	0.03174702	0.0757474	0.4047476
	MRE (η)	0	4.220842	0.086867	0.323435
	MRE (y_0)	0	0.036976	0.018483	0.043924

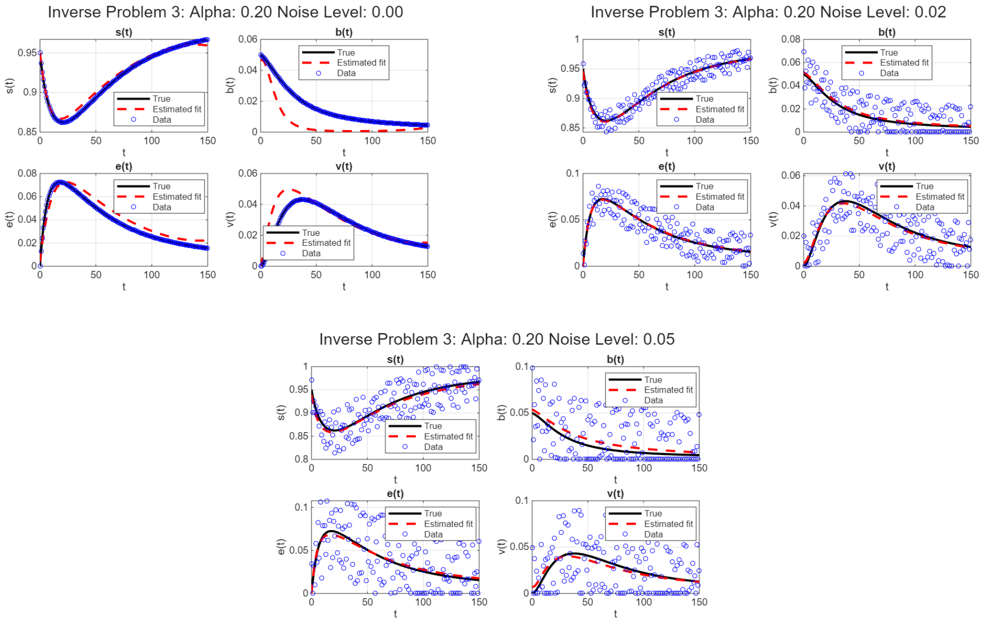

Figure 8: Numerical trajectories for **IP3** in the **threshold case** corresponding to the three noise levels $\zeta = 0$, 0.02, and 0.05.

Table 9: Recovered parameters and initial conditions in **IP3** for **endemic case** (where $\alpha/\gamma > 1$ in θ^{true}) under different noise levels.

		Noise Level:	0	0.02	0.05
	$\theta = (\eta, y_0)$	θ^{true}	$\widehat{\theta}$	$\widehat{\theta}$	$\widehat{\theta}$
η	α	0.4	0.400007	0.407267	0.420139
	β	0.30	0.299999	0.292655	0.281626
	γ	0.20	0.200003	0.203498	0.209698
	ε	0.10	0.100000	0.097815	0.094492
	δ	0.05	0.050000	0.049887	0.049819
	λ	0.07	0.070000	0.070555	0.071560
y_0	s_0	0.95	0.949998	0.946759	0.940946
	b_0	0.05	0.049999	0.050060	0.049907
	e_0	0.00	0.000003	0.000000	0.000394
	v_0	0.00	0.000000	0.003181	0.008753
	$J(\theta)$	0	0.000000	0.08080608	0.5035087
	MRE (η)	0	0.00000597	0.01536323	0.04017831
	MRE (y_0)	0	0.00001105	0.00230579	0.00569526

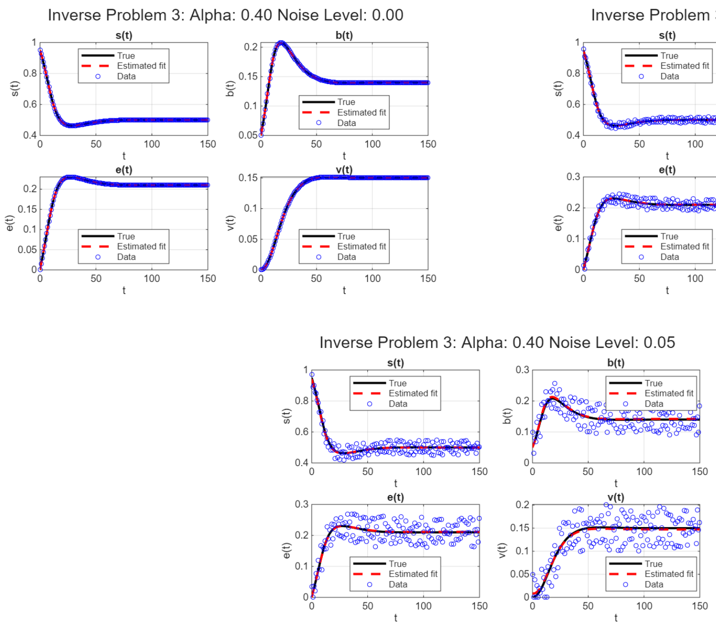

Figure 9: Numerical trajectories for **IP3** in the **endemic case** corresponding to the three noise levels $\zeta = 0$, 0.02, and 0.05.

4. Discussion of Numerical Results

The numerical experiments show that the proposed inverse framework is capable of recovering unknown quantities from observational data; however, the quality of recovery depends strongly on the dynamical scenario of the bullying model and on the type of inverse problem under consideration. Overall, the results in Tables 1-9 and Figures 1-9 reveal a clear distinction between parameter identification, initial-state reconstruction, and simultaneous recovery.

For IP1, where only the transition parameters are unknown, the reconstruction is highly accurate in the noise-free case, but becomes increasingly sensitive to noise in the non-bullying and threshold scenarios. This behavior is evident in Tables 1 and 2, where the recovered values may deviate substantially from the true ones when the noise level increases. Figures 1 and 2 show that even when the computed trajectories remain visually close to the data, the recovered parameters themselves may not be reliable. By contrast, Table 3 and Figure 3 show that in the endemic scenario the parameter recovery is noticeably more stable, even in the presence of noise. Thus, for IP1, the numerical results indicate that practical identifiability is strongly scenario-dependent. From a mathematical point of view, this behavior is consistent with the role of the threshold ratio (3.2). From the perspective of nonlinear dynamics, the present results reveal that the identifiability of the inverse problem is strongly linked to the qualitative regime of the underlying system. In particular, near the critical threshold $R_0 \approx 1$, the system exhibits a form of dynamical indistinguishability, whereby different parameter configurations produce nearly identical observable trajectories. This behavior reflects a loss of practical identifiability associated with critical transitions, and can be interpreted as a nonlinear phenomenon arising from the balance between competing mechanisms governing the system dynamics. In contrast, in the endemic regime, the persistence of bullying generates a more distinct dynamical signature, leading to improved parameter distinguishability. Near the critical scenario, the observed dynamics are influenced more by the balance between the bullying transmission and recovery effects than by the individual values of α and γ taken separately. As a consequence, different parameter vectors may produce very similar trajectories for $s(t)$, $b(t)$, $e(t)$, and $v(t)$. This explains why the inverse problem becomes practically ill-conditioned near the threshold case and, to some extent, also in the non-bullying scenario under noisy observations. In contrast, in the endemic scenario the sustained persistence of bullying creates a clearer dynamical signature, which improves parameter distinguishability.

From an educational perspective, this is an important message. In real school settings, similar observed bullying trends do not necessarily imply similar underlying mechanisms. Two schools may display comparable time profiles for bullying prevalence, while the hidden causes are quite different. In one setting, the dominant issue may be a strong peer-driven transition into bullying; in another, the main difficulty may be weak recovery due to ineffective intervention or insufficient institutional response. The results for IP1 therefore suggest that school data should not be interpreted only at the surface level. Instead, inverse analysis can help distinguish between school environments that look similar in terms of outcomes but differ substantially in the mechanisms driving those outcomes. A second important observation is that the threshold scenario is not only mathematically delicate, but also educationally meaningful. It corresponds to a school environment that is close to a tipping point: bullying is neither clearly dying out nor clearly persisting. In such circumstances, relatively small changes in supervision, counseling quality, peer influence, parental involvement, or intervention timing may shift the system toward either improvement or deterioration. The numerical difficulties observed in Table 2 and Figure 2 therefore have a natural educational interpretation: the most sensitive school environments may also be the hardest to analyze reliably from noisy data. This is precisely the type of situation in which educational decision-makers should be cautious, since policy choices may be highly consequential even when the available data do not allow precise estimation of all model parameters.

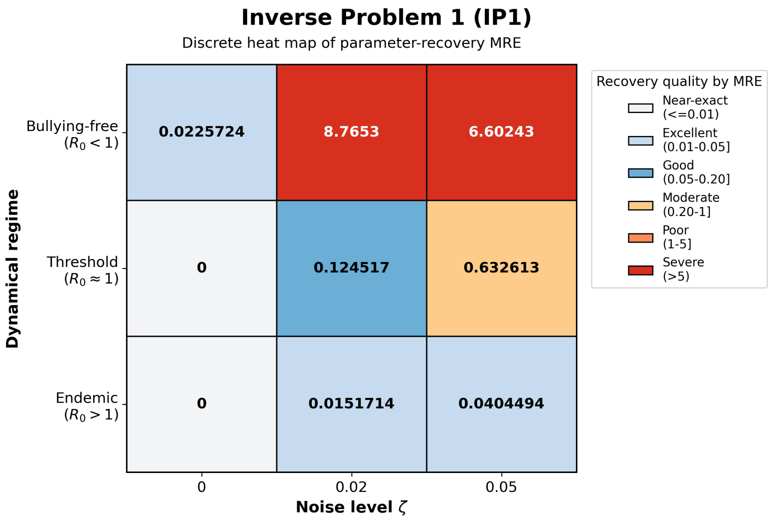

Figure 10: Discrete heat map for IP1 showing the mean relative error (MRE) of parameter recovery across dynamical regimes and noise levels. The results highlight severe instability in the bullying-free and threshold regimes under noise, while the endemic regime remains robust.

Compared with IP1, the second inverse problem is noticeably more stable. When the transition parameters are assumed to be known, the initial population proportions can be reconstructed with good accuracy across all three scenarios. This is evident from Tables 4-6, where the mean relative errors remain small, and from Figures 4-6, which show good agreement between reconstructed and observed trajectories. This indicates that, for the present model, the recovery of the initial state is better conditioned than the estimation of transition parameters. This finding also has a useful educational interpretation. If schools or researchers already possess reasonable estimates of the main transition rates; for example, from previous studies, institutional experience, or calibrated longitudinal datasets–then the model can be used to infer the initial distribution of students across the susceptible, bullying, exposed, and violent categories with comparatively high confidence. In practical terms, this means that inverse modeling may help schools reconstruct the hidden initial composition of a student population even when that composition is not directly measurable. Such information may be valuable for the early design of intervention programs, because it helps identify whether a school begins from a mostly susceptible population, from a setting with an already established bullying presence, or from a more fragile exposed/violent configuration requiring rapid support measures.

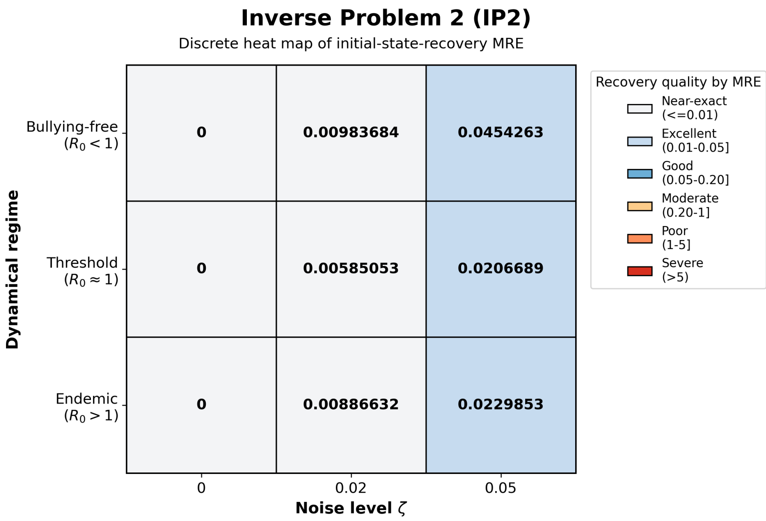

Figure 11: Discrete heat map for IP2 showing the mean relative error (MRE) of initial-state recovery. The reconstruction remains uniformly accurate across all regimes, indicating that initial-state estimation is better conditioned than parameter identification.

The most realistic case is IP3, where both the transition parameters and the initial conditions are unknown and must be estimated simultaneously. As expected, this problem is more challenging. Tables 7–9 and Figures 7–9 show that simultaneous recovery remains very accurate in the endemic scenario and is still acceptable in some noisy cases, but deteriorates more significantly in the threshold scenario. In the threshold regime of IP3, the noise-free case already exhibits a nonzero objective value and a poor recovery of the true parameters. Since the data are noise-free, this indicates convergence to a local minimum rather than the global one. This numerical anomaly reflects the practical non-identifiability of the model near the threshold, where distinct parameter sets can generate similar trajectories, and shows that even 400 MultiStart points do not guarantee global convergence in this regime. In particular, Table 8 shows that a good fit between reconstructed trajectories and observed data does not necessarily imply accurate parameter identification. Thus, inverse modeling in this setting should be viewed not only as an estimation tool, but also as a diagnostic tool indicating when the available data are insufficient for reliable parameter recovery. This point is especially important for educational readers. In applied school contexts, administrators may be tempted to trust a model simply because its curves fit the observed data well. However, the results of IP3 show that a visually good fit does not automatically mean that the inferred mechanisms are correct. This is a valuable warning for educational research and policy: model-based conclusions should not be judged solely by predictive agreement, but also by whether the available data are rich enough to support reliable interpretation. In this sense, inverse modeling can serve not only as an estimation tool, but also as a diagnostic tool indicating when the available evidence is insufficient for strong claims.

To further synthesize the numerical findings across all inverse problems, we summarize the reconstruction performance using discrete heat map representations. These discrete heat maps condense the numerical evidence of Tables 1-9 into a unified regime-noise stability landscape. They clearly show that identifiability is not uniform across the model's dynamical regimes: parameter recovery in IP1 and in the parameter block of IP3 deteriorates sharply in the bullying-free and near-threshold cases under noisy observations, whereas the endemic regime remains significantly more distinguishable and stable. By contrast, IP2 exhibits consistently high accuracy across all regimes, indicating that the reconstruction of initial conditions is substantially better conditioned than the recovery of transition parameters. This contrast highlights a fundamental structural feature of the inverse problems under consideration, namely that sensitivity to noise is strongly amplified near critical dynamical transitions. In this way, the heat map representations provide a compact and visually transparent confirmation of the central message of this work: practical identifiability is governed not only by the noise level in the data, but also, and more importantly, by the qualitative regime of the underlying nonlinear dynamics. These observations are clearly illustrated in Figures 10-12.

The numerical results also suggest a substantive interpretation of the parameters for educators and policy-oriented readers. The parameter α may be viewed as a proxy for the social reinforcement of bullying behavior, while γ measures the strength of interrup-

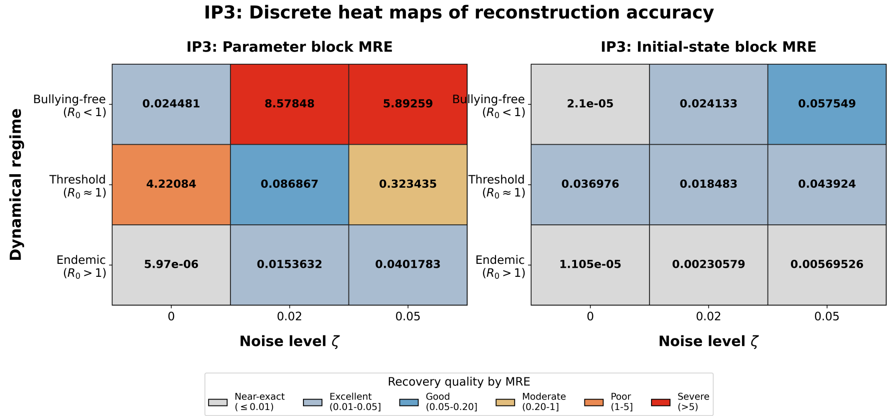

Figure 12: Discrete heat maps for IP3 showing the mean relative error (MRE) for simultaneous recovery of parameters and initial conditions. The parameter block is highly sensitive in the bullying-free and threshold regimes, whereas the endemic regime remains stable. Initial-condition recovery is comparatively robust across all scenarios.

tion, correction, or recovery. Likewise, β reflects the rate at which susceptible students become affected without becoming active bullies, whereas δ and λ describe escalation and de-escalation in the exposed and violent pathways. Under this interpretation, the inverse problems studied here are not merely technical reconstruction tasks; they correspond to estimating hidden features of school climate, including how rapidly harmful behavior spreads, how effectively it is contained, and how easily victimization escalates into more severe responses. This gives the model clear educational relevance, since such quantities are closely related to prevention planning, intervention design, and program evaluation. Another educational message emerging from Tables 1-9 and Figures 1-9 is that the usefulness of school data depends not only on noise level, but also on the structural informativeness of the scenario itself. Endemic bullying leaves a stronger dynamical footprint in the data, so the inverse problem is easier. Near the threshold, by contrast, the underlying mechanisms may remain partially hidden even when the observed trajectories appear regular and well behaved. Thus, educational datasets should not be judged only by sample size or by measurement precision, but also by whether the observed school dynamics are informative enough to distinguish competing explanations. This is an important contribution of the present study: it shows not only what can be estimated from school-level data, but also what may remain uncertain.

Overall, this study leads to two main conclusions. Mathematically, it clarifies that the inverse problems are stable in some scenarios and practically ill-conditioned in others, especially near the critical threshold. Educationally, it shows that inverse problem methodology provides a promising bridge between observable school data and hidden transition mechanisms that are difficult to measure directly. Such a framework may help researchers and practitioners interpret bullying data more carefully, identify schools that are close to critical behavioral transitions, and design interventions that are better aligned with the actual mechanisms operating in the school environment. In summary, the study shows that inverse problem techniques provide a useful framework for linking observable data with underlying mechanisms in bullying dynamics, while also highlighting the limitations that arise in sensitive dynamical regimes.

5. Conclusion

In this work, we studied three inverse problems for a compartmental model of bullying dynamics: the reconstruction of transition parameters, the reconstruction of initial conditions, and their joint recovery from synthetic observations, denoted by IP1, IP2, and IP3. The numerical results show that the proposed least-squares and MultiStart framework performs well in the noise-free case and remains reasonably robust under moderate noise, especially in the endemic regime. At the same time, the results reveal substantial practical identifiability difficulties near the threshold regime, where distinct parameter configurations may generate very similar observable trajectories. In particular, the joint reconstruction problem is the most challenging, and even in the noise-free threshold case the optimization may converge to a local minimum rather than the global one. These findings indicate that inverse modeling in this setting should be viewed not only as an estimation tool but also as a diagnostic tool for assessing whether the available data support reliable parameter recovery.

A limitation of the present study is that the numerical experiments assume full observability, i.e., all four state variables are available at all observation times. While this provides a useful baseline for assessing the intrinsic reconstruction properties of the inverse problems, it is clearly an idealized setting. In practical school-based applications, some compartments, especially the exposed class, may be only partially observed or not directly observable. We also performed preliminary tests with Tikhonov-type regularization and additional penalties involving α/γ and $\alpha-\gamma$, but in the limited experiments considered these modifications did not produce a clear improvement in reconstruction quality. Extending the inverse analysis to partial-observation settings and carrying out a more systematic study of regularization strategies therefore remain important directions for future work.

Acknowledgements

The authors sincerely thank the anonymous referees and the editor for their insightful comments and constructive suggestions, which have significantly enhanced the clarity and presentation of the manuscript.

References

[1] N. Crokidakis. A mathematical model for the bullying dynamics in schools. *Applied Mathematics and Computation*, 492:129254, 2025.

[2] D. O'Regan. Existence theory for nonlinear ordinary differential equations. *Kluwer Academic, Dordrecht*, 1997.

[3] C. Jacobson. R. Bronson. Modeling the dynamics of social systems. *Computers & Mathematics with Applications*, 19:35–42, 1990.

[4] S. Galam. Sociophysics: A physicist's modeling of psycho-political phenomena. *Springer, Berlin*, 2012.

[5] N. Crokidakis M. Perc. M. G. E. da Luz, C. Anteneodo. Sociophysics: social collective behavior from the physics point of view. *Chaos, Solitons & Fractals*, 170:113379, 2023.

[6] D. Olweus. Annotation: bullying at school: basic facts and effects of a school-based intervention program. *Journal of Child Psychology and Psychiatry*, 35:1171–1190, 1994.

[7] W. Liu et al. Prevalence, risk factors, and consequences of school bullying. *BMC Public Health*, 2025.

[8] D. Olweus. Bully/victim problems in school: facts and intervention. *European Journal of Psychology of Education*, 12:495–510, 1997.

[9] D. Olweus. School bullying: development and some important challenges. *Annual Review of Clinical Psychology*, 9:751–780, 2013.

[10] D. M. G. Comissiong. J. Sooknanan. When behaviour turns contagious: the use of deterministic epidemiological models in modeling social contagion phenomena. *International Journal of Dynamics and Control*, 5:1046–1050, 2017.

[11] D. M. G. Comissiong. J. Sooknanan. A mathematical model for the treatment of delinquent behaviour. *Socio-Economic Planning Sciences*, 63:60–69, 2018.

[12] E. Bellodi M. Gavanelli M. Bresadola. J. Franceschi, L. Pareschi. Modeling opinion polarization on social media: application to covid-19 vaccination hesitancy in italy. *PLOS ONE*, 18(10):e0291993, 2023.

[13] S. Galam. M. A. Javarone. Modeling radicalization phenomena in heterogeneous populations. *PLOS ONE*, 11(5):e0155407, 2016.

[14] F. Bu. Y. Wang. Modeling radicalization of terrorism under the influence of multiple ideologies. *AIMS Mathematics*, 7:4833–4850, 2022.

[15] N. Crokidakis. Radicalization phenomena: phase transitions, extinction processes and control of violent activities. *International Journal of Modern Physics C*, 34:2350100, 2023.

[16] World Health Organization. One in six school-aged children experiences cyberbullying, finds new who/europe study. *WHO Report*, 2024.

[17] D. P. Farrington. M. M. Ttofi. Effectiveness of school-based programs to reduce bullying: a systematic and meta-analytic review. *Journal of Experimental Criminology*, 7:27–56, 2011.

[18] A. Angold E. J. Costello. D. Wolke, W. E. Copeland. Impact of bullying in childhood on adult health, wealth, crime, and social outcomes. *Psychological Science*, 24(10):1958–1970, 2013.